Radiative feedbacks of dust-in-snow over East Asia in CAM4-BAM

Xiaoning Xie[1], Xiaodong Liu[1,2], Huizheng Che[3], Xiaoxun Xie[1], Xinzhou Li[1], Zhengguo Shi[1], Hongli Wang[4], Tianliang Zhao[5], and Yangang Liu[6]

[1]SKLLQG, Institute of Earth Environment, Chinese Academy of Sciences, Xi'an 710061, China
[2]University of Chinese Academy of Sciences, Beijing 100049, China
[3]Key Laboratory for Atmospheric Chemistry, Institute of Atmospheric Composition, Chinese Academy of Meteorological Sciences, CMA, Beijing 100081, China
[4]Shaanxi Radio and TV University, Xi'an 710119, China
[5]Key Laboratory for Aerosol-Cloud-Precipitation of China Meteorological Administration, Nanjing University of Science Information &Technology, Nanjing 210044, China
[6]Environmental and Climate Sciences Department, Brookhaven National Laboratory, Upton, NY 11973-5000, USA

Correspondence to: Xiaoning Xie (xnxie@ieecas.cn)

Abstract. Dust-in-snow on the Tibetan Plateau (TP) could reduce the visible snow albedo by changing surface optical properties and removing the snow cover through increased snowmelt, which leads to a significant positive radiative forcing and remarkedly alters the regional energy balance and the East Asian climate system. This study extends our previous investigation in dust-radiation interactions to investigate the dust-in-snow radiative forcing (SRF) and its feedbacks on the regional climate and the dust cycle over East Asia by use of the Community Atmosphere Model version 4 with a Bulk Aerosol Model parameterization of the dust size distribution (CAM4-BAM). Our results show that SRF increases the East Asian dust emissions significantly by 13.7% in the spring, countering a 7.6% decrease in the regional emissions by the dust direct radiative forcing (DRF). SRF also remarkedly enhances the whole dust cycle, including transport and deposition of dust aerosols over East Asia. The simulations indicate an increase in dust emissions of 5.1% due to the combined effect of DRF and SRF. Further analysis reveals that these results are mainly due to the regional climatic feedbacks induced by SRF over East Asia. By reducing the snow albedo over the TP, the dust-in-snow mainly warms the TP to enhance its thermal effects by increasing the surface sensible and latent heat flux, which in turn increases the aridity and westerly winds over Northwest China and enhances the regional dust cycle. Additionally, the dust-in-snow also accelerates snow melting, reduces the snow cover, and then expands the East Asian dust source region area, which results in increasing the regional dust emissions. Hence, a significant feature of SRF on the TP can create a positive feedback loop to enhance the dust cycle over East Asia.

1 Introduction

A large amount of desert dusts from East Asia arid and semi-arid regions are emitted into the atmosphere, which can be carried over the wide downwind regions including the eastern China and the Pacific Ocean, and also deposited in snow over the Tibetan Plateau (Wake et al., 1994; Zhang et al., 1997; Zhao et al., 2006). The dusts can significantly affect global and regional energy balance, climate, and hydrological cycle by dust direct radiative forcing and dust-in-snow radiative forcing (Ramanathan et al., 2001; Shao et al., 2011; Mahowald et al., 2014; Huang et al., 2014; Qian et al., 2015).

Dusts in the atmosphere can directly absorb and scatter the thermal (longwave) and solar (shortwave) radiation labeled as dust direct radiative forcing (DRF). Note that the importance of DRF in general circulation models (GCMs) has been recognized for many years (Tegen and Lacis, 1996; Miller and Tegen, 1998; Yue et al., 2009; Mahowald et al., 2014). On the global scale, the dust DRF is about -0.4 W m^{-2} with a range between -0.30 and -0.6 W m^{-2} estimated by the current models described by Huneeus et al. (2011), as reviewed by Kok et al. (2017). The DRF with particle size distribution for dust from Kok (2011) is less cooling (smaller forcing) because atmospheric dust is coarser than represented in current models. The new size distribution results in DRF range of -0.48 Wm^{-2} and +0.2 W m^{-2}, including the possibility that dust causes a net warming of the planet (Kok et al., 2017). The regional DRF over Asia is significantly higher than that at the global scale due to the larger dust loading, influencing the regional climate (Lau et al., 2006; Zhang et al. 2009; Han et al. 2012; Sun et al., 2012; Guo and Yin et al., 2015; Gu et al., 2016). A so-called Elevated Heat Pump effect due to atmospheric heating by elevated absorbing aerosols strengthens large-scale atmospheric circulation and enhances the precipitation in the late boreal spring and early summer season over the foothills of the Himalayas and northern India (Lau et al., 2006). The aerosol-heating reduces the Tibetan and Himalayan snowpack cover by $6-10\%$, neglecting the greenhouse warming (Lau et al., 2010). The net surface and TOA radiative fluxes are decreased by DRF and cause a surface cooling over East Asia and increase the regional local stability (Zhang et al., 2009). Dust loading in spring and summer alerts the East Asian summer monsoon through affecting atmospheric circulation and thermal structures induced by DRF (Sun et al., 2012; Guo and Yin, 2015). Gu et al. (2016) claimed that the circulation and precipitation responses to DRF are different over South/East Asia and North Africa, which is dependent on the relative location of dusts to the rainfall band.

Depositions of light absorbing aerosols on snow (e.g., black carbon and dust) can reduce the visible snow albedo by changing surface optical properties and remove snow cover by increasing snowmelt in entirely or partially snow covered areas, resulting in a significant positive radiative forcing (Hansen and Nazarenko, 2004; Xu et al., 2009; Huang et al., 2011; Qian et al., 2015). Based on previous studies (Hansen and Nazarenko, 2004; Hansen et al., 2005), IPCC (2007) showed the radiative forcing range of 0.10 ± 0.10 W m^{-2} induced by aerosol-in-snow at the global scale, whereas IPCC (2013) adopted a radiative forcing of +0.04 (+0.02 to +0.09) W m^{-2} according to results of Bond et al. (2013). Recent studies have shown the significant impacts of snow grain shape (spherical vs. nonspherical) and aerosol-snow mixing state (internal vs. external) on BC/dust-in-snow radiative forcing (e.g., Flanner et al., 2012; Liou et al., 2014; Dang et al., 2016; He et al., 2017b, 2018a). Further studies also shown the effects of snow grain packing (He et al., 2017a) and aerosol size distribution in snow (Schwarz et al., 2013; He et al., 2018b) on aerosol-snow interactions. The Tibetan Plateau (TP) is a vast elevated plateau with an average elevation of 4,

500 meters, located in Asia (Figure 1). In addition to being close to the Taklamakan (one of the largest sand deserts in the world) and Gobi deserts, the TP also has several deserts (e.g., Qaidam Basin desert) within it and is near the industrial regions in Indian subcontinent and eastern China. There exists a larger amount of deposition on snow of black carbon and dust aerosols over the TP due to the high industrial and natural emissions in Asia from observational studies (Xu et al., 2009; Ming et al., 2013; Qu et al., 2014; Lee et al., 2017; Li et al., 2018; Zhang et al., 2018). Over this region, the particles of dusts are the dominant insoluble impurities compared with black carbon in terms of particle mass (Ming et al. 2013; Qu et al., 2014). These studies further claim that the impact of dust aerosols on snow albedo and dust-induced surface radiative forcing exceed those of black carbon over the TP, mainly because of larger dust loading. The aerosol-induced snow albedo perturbation generates much larger positive surface radiative flux changes with $5-25$ W m^{-2}, during spring over the TP (Flanner et al., 2009; Qian et al., 2011). Furthermore, Qian et al. (2011) claimed that absorbing aerosol in snow can cause a 1.0°C warming over the TP, which can influence the East Asian and South monsoon through the TP's thermal and dynamical forcing.

Dust cycles, including dust emissions, transports, as well as dry and wet depositions, are altered by DRF through affecting the atmospheric vertical thermal structures and surface wind speed. The mechanism of PBL (the planetary boundary layer) (Miller et al., 2004; Perez et al., 2006; Heinold et al., 2007) was firstly proposed to explain the reduction of dust emissions induced by DRF (Perlwitz et al., 2001). It was described that the surface negative net DRF by dusts reduces the turbulent flux of surface sensible heat and reduces PBL mixing. A positive feedback between DRF and dust emissions are shown through the PBL mechanism over North Africa due to the surface positive net DRF. An alternative mechanism was proposed that DRF produces an anomaly in the surface pressure, especially on the edge of the dust layer, resulting in impacts on the circulation and wind speed (Ahn et al.,2007; Heinold et al., 2008).

In our previous study (Xie et al., 2018), we have shown using the improved Community Atmosphere Model version 4 with a Bulk Aerosol Model parameterization of the dust size distribution (CAM4-BAM) that DRF decreases the East Asian dust cycle owing to the negative surface radiative forcing through the PBL mechanism, which is opposite to the enhancement of North African dust emissions induced by DRF. Considering that the dust cycle change by the dust-in-snow radiative forcing (SRF) over East Asia has not been studied previously. Using the identical CAM4-BAM model, we extend the the DRF effects (Xie et al., 2018) to systematically to investigate the SRF, the regional climate change and the dust cycle change induced by the SRF over East Asia, and also compare with the DRF effects discussed in Xie et al. (2018). The rest of this paper is structured as follows. In Section 2, we first review the improved CAM4-BAM model based on Albani et al. (2014) and Xie et al. (2018), and describe the experimental design. The model performance is also evaluated against the temporal and spatial observations of snow cover and surface temperature. The model results for dust radiative forcing and its radiative feedbacks are discussed for the area of study in Section 3. Further discussions and conclusions are summarized in Sections 4 and 5, respectively.

2 Model evaluation and experimental design

2.1 CAM4-BAM and experiments

The CAM4 model described in detail by Neale et al. (2010) is the atmospheric component of the Community Climate System Model version 4 (CCSM4). The CAM4-BAM model considers a subbin fixed size distribution of externally mixed sulfate, sea salt, organic carbon, black carbon, and dust by Tie et al. (2005). The improvements to CAM4-BAM for the dust cycle was proposed based on three major aspects including the optimized soil erodibility maps with respect to each of the macroareas, updated optical properties of dusts with realistic absorption parameters, and a new size distribution for dust emissions, which has a better representation of the dust cycle, most notably for the improved size distribution (Albani et al., 2014). The new size distribution decreases the emitted fraction of clay aerosols (<2 μm) in excellent agreement with measurements and exerts a smaller cooling compared released version. This improved model can be used to investigate the East Asian dust cycle and the DRF over this region (Xie et al., 2018). Black carbon and mineral dust in snow were represented in the Snow, Ice, and Aerosol Radiative (SNICAR) component (Flanner et al., 2007; 2009), which has been used to investigate the aerosol-in-snow forcing at the global scale (Flanner et al., 2009) and at the regional scale (Qian et al., 2011). Note that a set of new parameterizations including the effects of snow grain shape and aerosol-snow mixing state has been coupled into the SNICAR model, which may represent the realistic snowpack situation (He et al., 2018c). It is interesting to check the difference in radiative forcing between these two models in the future.

In this work, the improved CAM4-BAM model adopts the finite volume (FV) scheme for the dynamical core with a higher horizontal resolution ($0.9^\circ \times 1.25^\circ$), and with 26 levels in the vertical direction. All the model simulations were run for the year 2000 and constrained with the sea surface temperature (SST), sea-ice concentrations, and atmospheric forcings including solar irradiance, tropospheric and stratospheric ozone, and greenhouse gases during this period. The SST and sea-ice concentration were from a merged version of the HadISST (Rayner et al., 2003) and the optimum interpolation SST data sets described by Hurrell et al. (2008). We conducted three numerical experiments including 21-year free run with a 1-year spin up (no nudging), one with both DRF and SRF (Case1), one with the DRF and without the SRF (Case2), the other one without the DRF and the SRF (Case3), as summarized in Table 1. It is noted that, here we only consider the dust aerosols in these three numerical experiments, and neglect the radiative properties of other aerosols including sulfate, sea salt, organic carbon and black carbon in the improved CAM4-BAM model. Based on these three experiments including Case 1, Case 2, and Case 3, we can derive the DRF (Case2$-$Case3), the SRF (Case1$-$Case2), and the total radiative forcing (DRF+SRF, Case1$-$Case3). Hence, we use the results of the differences between these three experiments to investigate the climatic feedback of SRF and the dust cycle changes induced by SRF over East Asia, also as compared with changes induced solely by DRF. Due to the complex topography of the TP, higher-resolution simulations can resolve more details of the deep valleys and high mountains over and around the TP and make some significant improvements in the simulated climate (Li et al., 2015). Hence, it is necessary to conduct the higher-resolution simulations to address this issue.

2.2 Model evaluation

This subsection assesses the climatological features including the simulated dust aerosol optical depth at 550 nm (AOD), dust deposition, snow cover and surface temperature in order to evaluate the impacts of dust-in-snow forcing over the TP. Figure 2a shows the monthly dust AOD over the TP from the CAM4-BAM model. It shows that the dust AOD has the largest values (> 0.06) in MAM (March-April-May), likely because of the higher frequency of dust storms over this region in MAM. Figure 2b displays the spatial distribution of the simulated MAM dust AOD from CAM4-BAM. This simulated spatial distribution shows that the dust AOD has larger values over dust source regions (Gobi and Taklamakan deserts), where dust AOD are greater than 0.2 particularly over the Taklamakan desert. Figure 2c shows the monthly mean dust deposition over the TP including dry, wet and total (dry+wet) depositions, indicating the largest dust deposition in MAM. This phenomenon of the monthly variation of dust deposition is very similar with the dust AOD (Figure 2a). It is noted that the dry deposition of dusts is much larger than the wet deposition probably because of less rain over Northwest China and its seasonal precipitation (Lau et al., 2006; Xu et al., 2008; Kang et al., 2010). Figure 2d shows that the total dust deposition exhibits two peaks over the two dust source regions. Additionally, deserts in the western and northeastern regions of TP exhibit peaks in dust deposition, which we expect to further increase the SRF signal. This improved CAM4-BAM has been evaluated against measurements such as AOD, and dust deposition over the East Asia (Albani et al., 2014; Xie et al., 2018), showing a better simulation of dust cycle.

Figure 3 shows the monthly mean snow cover fraction (SCF) and surface temperature over the TP from the model and observations (MODIS SCF and CRU (Climatic Research Unit) surface temperature data). The MODIS data shows a larger SCF in the winter and spring over the TP, with the maximum reaching approximately 25% in January (Figure 3a). The corresponding minimum SCF occurs in July and August. Overall, the CAM4-BAM model can capture the monthly variations of SRF, with the minimum in summer and maximum in winter and spring. But, the model overestimates the amplitude of the monthly variations of SCF, with overestimated SCF in winter and spring and underestimated SCF in summer. The overestimated SCF variation is due probably to the model's coarse horizonal resolution ($0.9^\circ \times 1.5^\circ$) and smooth terrain (Qian et al., 2011; Lee et al., 2013). Figure 4a shows that the MAM persistent snow covered areas with SRF $> 50\%$ are located in the western TP (including Pamir Plateau, Tianshan, and Kunlun mountains), the southeast TP (Hengduan mountain), Himalayas mountain, and Qilian mountain. The model can capture these most persistent snow covered areas (Figure 4b). In contrast to the case of SCF, the data from the Climatic Research Unit (CRU) shows a lower surface temperature in winter and spring, and a higher surface temperature in summer (Figure 3b). Furthermore, the CAM4-BAM model can better capture the spatial distribution (Figure 4c) and the monthly variations of the surface temperature (Figure 4d), although it also overestimates the amplitude of monthly variations in the surface temperature.

3 Dust radiative forcing and its radiative feedbacks

3.1 Dust cycle changes induced by SRF

It has been well recognized that mineral dusts can influence the atmospheric vertical thermal structures and surface wind speed by DRF, which affects the dust cycle through various mechanisms (Perlwitz et al., 2001; Miller et al., 2004; Perez et al., 2006; Heinold et al., 2007; Ahn et al., 2007; Heinold et al., 2008; Colarco et al., 2014; Xie et al., 2018). However, the dust cycle change induced by the SRF over East Asia has not been systematically studied previously, despite reported large surface positive SRF over the TP (Flanner et al., 2009; Qian et al., 2011). This subsection fills this gap to examine the SRF-induced dust cycle changes during MAM over East Asia, including dust emissions, dust transport (defined as the vertically integrated dust flux, which is similar to water vapor transport), and the dry and wet depositions. Comparison with the DRF is also made to estimate their relative contributions.

Figure 5 shows the spatial distribution of the dust cycle changes induced by DRF (left column), SRF (middle column), and the total radiative forcing (DRF+SRF, right column) over East Asia in MAM; the corresponding averaged values are summarized in Table 2 over the East Asian dust source area (75°E−115°E and 25°N−50°N). Figures 5a shows that DRF decreases the dust emissions over this region by -8.8 Tg season^{-1}, with a magnitude of -7.6% in Table 2. The corresponding dust transport, dry and wet depositions in Figures 5d, 5g and 5j are also decreased over this region by DRF, with the magnitudes of -6.4%, -5.7%, and -1.8%, respectively. Figure 5b shows that SRF markedly enhances the dust emissions over the East Asian dust source area, with 14.78 Tg season^{-1} (13.7%), which is statistically significant. It is noted that the changes of the dust emissions induced by SRF are approximately 2 times larger than that by DRF. The changes of dust transport, dry and wet depositions (Figures 5e, 5h, and 5k) are also enhanced by SRF with 6.9%, 11.9%, and 4.7%, respectively.

Figures 5c, 5f, 5i and 5l show the changes in dust cycle induced by the dust total radiative forcing. The dust emissions are significantly enhanced (in Figure 5c) by the dust total radiative forcing over East Asia by 5.1% with an increase of 5.98 Tg season^{-1}. It is noted that the total change in dust emissions induced by SRF+DRF is 5.98 Tg season^{-1}, which is absolutely exact. However, the changes caused by DRF (-8.8 Tg season^{-1}) and SRF (14.78 Tg season^{-1}) are included the nonlinear interactions between SRF and DRF. Hence, the values of dust emissions caused by DRF and SRF can be altered when removing the nonlinear interactions between SRF and DRF. That is because the changes of dust emissions induced by the SRF are much larger than that by the DRF. The dry and wet depositions are also increased (5.5% and 2.9%) in Figure 5i and 5l by the dust total radiative forcing. Figure 5f shows the dust transport is enhanced over the northern region of the East Asian dust source region although the averaged value of the dust transport is slightly decreased by -0.9% (shown in Table 2) over this region due to the decreased dust transport over the southern region. In summary, the dust total radiative forcing enhances the dust cycles, because the SRF-induced enhancement is much stronger than the diminishment caused by DRF.

3.2 Dust radiative forcing and the dust-induced changes in surface properties

It is noted that these dust cycle changes induced by the DRF, the SRF and the dust total radiative forcing (Figure 5) are mainly due to the corresponding radiative forcing and its climatic feedbacks. This section examines the dust-induced radiative forcing including DRF and SRF and its climatic feedbacks, especially about the SRF.

Figure 6a shows the spatial distribution of the simulated surface albedo in MAM for Case 1. Evidently, there exists a larger broadband surface albedo over the TP, especially over the western TP due to larger SCF (Figure 4b). Compared to the MODIS surface albedo over the TP (Meng et al., 2018), the CAM4-BAM model captures its spatial distribution during MAM. However, the model overestimates the surface albedo, which is similar with multi-model ensembles' results (Li et al., 2016), mainly due to the overestimated SCF and the ignoring BC-in-snow. Dust-in-snow can decrease the snow albedo over entirely or partially snow covered areas as mentioned above. Figure 6b shows the dust-in-snow significantly reduces the broadband surface albedo over the TP and its surrounding mountains, especially over the western TP (reaching over -0.1). The decrease in snow albedo mainly results from a positive feedback process: absorbing aerosols deposited on snow $\rightarrow$ reducing surface albedo $\rightarrow$ increasing surface net solar radiation $\rightarrow$ increasing surface temperature $\rightarrow$ reducing snow fraction and depth $\rightarrow$ finally reducing surface albedo, which was proposed by Qian et al. (2011). Another element in this positive feedback process is that increasing surface temperature results in stronger snow aging and hence larger snow effective grain sizes, and finally reduces snow albedo (Flanner et al., 2009).

Figure 7 shows that the dust-induced changes in the surface radiative forcing and surface temperature in MAM by the DRF, the SRF and the total radiative forcing. The DRF displays a surface negative radiative forcing over East Asia, where it is much larger and statistically significant over the Taklamakan and Gobi deserts (Figure 7a). This is mainly because the high scattering efficiency of large amounts of dust aerosols over these two dust source regions exerts a larger surface negative radiative forcing. This surface negative radiative forcing reduces the surface sensible heat, and then decreases vertical mixing within the PBL and the wind speed at the surface, decreasing the regional dust emissions (labeled by the PBL mechanism) over East Asia (Xie et al., 2018). It is noted that this PBL mechanism was firstly shown and proved by Miller et al. (2004), Perez et al. (2006) and Heinold et al. (2007). Figure 7b shows the surface temperature is also decreased slightly between -1°C to 0°C over East Asia, likely because of the surface negative radiative forcing.

In contrast, Figure 7c shows that SRF displays a significant surface positive radiative forcing over the whole TP and the surrounding mountains, especially over the western TP (above 20 W m^{-2}). The decreased surface albedo over the TP (Figure 6b) causes increasing surface net solar radiation and shows a surface positive radiative forcing over this region. This positive surface radiative forcing significantly warms the whole TP, especially the western TP (beyond 2°C) in Figure 7d. Figure 7e shows the dust total radiative forcing exerts a significant and larger surface positive radiative forcing over the whole TP, compared to a significant and smaller surface negative radiative forcing over the Taklamakan and the Gobi deserts. Over the TP, the SRF mainly dominates the total radiative forcing and the DRF determines the total radiative forcing over the deserts and the wide downwind regions. Hence, the surface temperature significantly increases over the TP due to the larger total positive

forcing in Figure 7f, which is determined by the SRF. Hence, we will focus on the changes in the surface properties induced by the SRF in the following sections.

Figure 8a shows the spatial distribution of the changes in the SCF induced by the SRF. The SCF is significantly decreased by the SRF over the whole TP and its surrounding mountains, where the maximum decrease of the SCF can reach above 15%. The warming TP (Figure 7d) due to dust-in-snow accelerates snow melting, reduces the snow cover, and then expands the dust source region area, resulting in enhancing the regional dust emissions. Figure 8b shows the significant increase in the surface latent heat flux (LHF) by the SRF. That is due to the increased soil moisture induced by the enhanced snowmelt over the TP. Additionally, the increased surface precipitation during spring and summer by the SRF also increases the soil moisture in the following subsection. The warming TP also increases the regional surface sensible heat flux (SHF) in Figure 8c. The surface total heat flux (LHF+SHF) shows a larger value over the TP, especially over the western TP (reaching over 10 W m^{-2}). Hence, dust-in-snow over the TP can warm the TP and enhance its thermal effects by increasing the surface LHF and SHF, thereby affecting the Asian climate. It is noted that SRF significantly increases the surface temperature, reduces the SCF and enhances the surface total heat flux (LHF and SHF) over the TP, which is absolutely same as the previous results (Qian et al., 2011). Due to the higher horizontal resolution of $\sim$1 degree in this study, our result shows the finer spatial distribution of changes in these properties, especially over the TP compared to Qian et al. (2011).

3.3 Dust-induced climatic feedbacks

It is known that the TP referred to as the Third Pole can influence the Indian and East Asian summer monsoon and inland precipitation through its dynamical and thermal effects (e.g., Boos and Kuang, 2010; Wu et al., 2012; Liu et al., 2013; Shi et al., 2014; Sha et al., 2015). Qian et al. (2011) claimed that the absorbing aerosols (especially the black carbon) in snow over the TP affects the East and South Asian monsoon climate and hydrological cycle by the enhanced TP thermal effects. Here, we concentrate on the enhanced TP thermal effects due to dust-in-snow on the climate over the arid and semiarid regions of Northwest China.

Figure 9 show the changes in the zonal wind component and the Omega (vertical velocity, Pa s^{-1}) in a vertical cross section at 75°E−115°E in MAM induced by the SRF. It shows the anomalous westerly wind over the north of the TP (mainly including Northwest China) and the anomalous easterly wind forced by the SRF over the south of the TP in Figure 9a, which are generally statistical significant over these two regions. This is because the enhanced TP thermal effect due to increasing the surface LHF and SHF induced by the SRF increases the south-north temperature gradient, resulting in a westerly wind anomaly over the north of the TP (Schiemann et al., 2009; Li and Liu, 2015). Additionally, we show the spatial distribution of the mid-level westerly winds (Figure 10a) and the surface wind speed (Figure 10b) over East Asia, indicating that the the mid-level westerly winds and the surface wind speed are also significantly increased over Northwest China. The mid-level westerly winds have been recognized as one of the major factors for the long-distance dust transport process to the North Pacific Ocean and to North America and beyond from East Asian dust sources (Wilkening et al., 2000; Guo et al., 2017), while the surface wind speed affects the dust emission rate by influencing the dust saltation process (Shao et al., 2011). Hence, the increased westerly wind enhances the dust emissions and dust transport, which in turn increases the magnitude of the whole

dust cycle. Additionally, the enhanced TP thermal effect induced by SRF enhances the upward vertical velocity over the TP and the downward vertical velocity over Northwest China (or intensifies subsidence) in MAM from the vertical distribution in Figure 9b, which is also shown in Figure 10c based on the spatial distribution. This result leads to the decreased surface precipitation over Northwest China and the enhanced surface precipitation over the TP in Figure 10d. Note that the enhanced TP thermal effect by SRF lasts from spring to summer, which has been shown in Figure 11. It shows the downward vertical velocity is enhanced in summer (Figure 11a), resulting in the significant decreased surface precipitation (Figure 11b) over the north of the TP, whereas the upward vertical velocity and the surface precipitation are both enhanced over the TP. Hence, the SRF significantly decreases the surface precipitation in spring and summer and then enhances the regional aridity in Northwest China, resulting in enhancing the regional dust emissions. In general, the dust-in-snow mainly warms the TP and then increases the aridity and westerly winds by the enhanced TP thermal effects, in turn enhancing the East Asian dust cycle.

4 Further discussions

Figure 12 shows the changes in the dust emissions by the SRF in other seasons including JJA, SON, and DJF compared to MAM. It shows that the dust emissions are all enhanced by the SRF in all the seasons (MAM: 14.78 Tg season^{-1}, JJA: 0.78 Tg season^{-1}, SON: 1.56 Tg season^{-1}, and DJF: 5.86 Tg season^{-1}). The enhancement of dust emissions in MAM induced by the SRF is much larger than that in other seasons, which can account for 64% of the annual total increase in dust emissions. This is mainly because the larger snow cover in MAM, along with the largest dust deposition exerts a significant radiative forcing, climatic feedbacks, and changes in dust emissions in this season. Therefore, it is quite reasonable to focus on the dust radiative forcing and its feedbacks on climate and dust cycle in MAM in our work.

The above results indicate the predominate causes for SRF enhancement of the dust cycle over East Asia and is illustrated in Figure 13. Dust aerosols emitted from East Asian source regions where precipitation is limited and deposited on snow over the TP. The dust-in-snow over the TP reduces the surface albedo (Figure 6b) and warms the TP (Figure 7d), and then increases the westerly winds (Figure 9a) and the surface wind speeds (Figure 9b) through enhancing the south-north temperature gradient and the aridity over Northwest China (Figures 10d and 11b) by intensified subsidence. The enhanced aridity and stronger westerly winds can increase the dust emissions, and enhance the whole dust cycle (Figures 5d, 5e, 5h, and 5k). Additionally, the dust-in-snow also accelerates snow melting, reduces snow cover (Figure 8a), and then expands the dust source region area, resulting in increasing the dust emissions. Hence, a significant feature of SRF over the TP can create a positive feedback loop to enhance the dust emissions (as summarized in Figure 13).

Similar to our previous study (Xie et al., 2018), we compare the changes in the East Asian dust cycle by the dust radiative forcing with the North African dust emissions. Table 3 shows that the dust emissions are significantly enhanced with 8.9% by the DRF over North Africa, through both the strengthened large-scale circulation and the PBL mechanism (Xie et al., 2018). The changes in dust emissions by the SRF are much smaller than that by the DRF over North Africa, mainly due to less snow cover and negligible SRF over this region (figures not shown). Therefore, the systematic comparative analysis reveals that the

change in dust cycle over North Africa is dominated by DRF (Table 3) whereas it is controlled by SRF over East Asia due to the existence of the TP, as shown in Table 2.

5 Concluding Remarks

A large amount of desert dusts from East Asia arid and semi-arid regions are deposited on snow over the Tibetan Plateau (TP). Furthermore, the dust-in-snow reduces the visible snow albedo by changing surface optical properties and removes the snow cover by increasing snowmelt, leading to a significant positive radiative forcing (labeled by SRF). SRF over the TP can influence the regional climate and dust cycle over East Asia through enhancing the TP thermal effects.

In this study, the improved CAM4-BAM model was used to investigate the SRF and its feedbacks on the climate system and the dust cycle over East Asia. The CAM4-BAM simulations show that SRF increases dust emissions in the spring by 14.78 Tg season^{-1} (13.7%), thus enhancing dust transport and deposition over East Asia. Compared to the decreased dust emissions by -8.80 Tg season^{-1} with -7.6% (through the PBL mechanism) induced by the dust direct radiative forcing (DRF), the increased effects on dust emissions by SRF are much more significant. Simulation results show that the total effects of DRF and SRF can increase the dust emissions by 5.98 Tg season^{-1} with 5.1%. Dust-in-snow reduces the albedo over the TP which warms the TP and enhances TP thermal effects and the regional dust cycle; increased sensible and latent heat fluxes from the surface result in increased aridity and westerly winds over North China. Additionally, the dust-in-snow also accelerates snow melting, reduces snow cover, and expands the dust source region area, resulting in increasing dust emissions. In general, a significant feature of SRF over the TP can create a positive feedback loop to enhance the dust cycle, which is summarized in Figure 13.

It is noted that black carbon (BC) deposited on snow over the TP mainly from South Asia and East Asia (Xu et al., 2009; Wang et al., 2015) also displays a significant positive forcing over this region (Flanner et al., 2009; Qian et al., 2011). Here, we only consider the radiative forcing of the dust-in-snow over the TP ignoring the radiative forcing of the BC-in-snow in our study. Due to neglecting BC and dust nonlinear interactions, the dust-in-snow radiative forcing might not be accurate. Additionally, the overestimated SCF in the MAM may also artificially increase the dust-in-snow radiative forcing. The overestimated radiative forcing may amplify its feedbacks on the East Asian climate and dust cycle. Additionally, we focus on the East Asian arid and semi-arid regions in order to investigate the dust cycle changes induced by SRF in this paper. Qian et al. (2011) pointed out that the radiative forcing of the absorbing aerosols can substantially influence the South and East Asian monsoon climate and the regional hydrological cycle through the TP thermal effects using the CAM3.1 model.

It is noted that the atmospheric dust burden and deposition rate of dusts were much higher (approximately from 2 to 4 times) during the Last Glacial Maximum (LGM) compared to current climate mainly due to increased winds speeds, and the decrease in intensity of the hydrological cycle, as well as the expansion of dust source areas (Mahowald et al., 2006; Maher et al., 2010; Albani et al., 2012). The increased dust-in-snow over the TP due to higher atmospheric dust loadings may show a much larger positive radiative forcing and more significantly create the positive feedback loop to enhance the dust cycle in LGM. Hence, we will investigate the SRF and its feedbacks on the East Asian climate and the dust cycle during the LGM in the future.

Data availability. All model results are archived on the cluster at the Institute of Earth Environment, Chinese Academy of Sciences, and available upon request. Please contact Xiaoning Xie (xnxie@ieecas.cn) for access.

Competing interests. The authors declare that they have no conflict of interest.

Acknowledgements. This work was jointly supported by National Key Research and Development Program of China (2016YFA0601904), the Strategic Priority Research Program of Chinese Academy of Sciences (XDA20070103) and the National Natural Science Foundation of China (41690115, 41572150). Z. Shi is supported by CAS "Light of West China" Program. Y. Liu is supported by the US Department of Energy's Atmospheric System Research (ASR) program. The data of CRU temperature is acquired from http://www.cru.uea.ac.uk/data and the data of MODIS snow cover is from https://nsidc.org/data/modis/data_summaries/#snow.

References

Albani, S., Mahowald, N. M., Delmonte, B., Maggi, V., Winckler, G.: Comparing modeled and observed changes in mineral dust transport and deposition to Antarctica between the Last Glacial Maximum and current climates, Clim. Dyn., 38, 1731–1755, doi:10.1002/2013MS000279, 2012.

Albani, S., Mahowald, N. M., Perry, A. T., Scanza, R. A., Zender, C. S., Heavens, N. G., Maggi, V., Kok, J. F., and Otto-Bliesner, B. L.: Improved dust representation in the Community Atmosphere Model, J. Adv. Model. Earth Syst., 06, 541–570, doi:10.1002/2013MS000279, 2014.

Ahn, H. J., Park, S. U., and Chang, L. S.: Effect of direct radiative forcing of Asian dust on the meteorological fields in east Asia during an Asian dust event period, J. Appl. Meteorol. Climatol., 46, 1655–1681, 2007.

Bond, T. C., Doherty, S. J., Fahey, D. W., Forster, P. M., Berntsen, T., Deangelo, B. J., Flanner, M. G., Ghan, S., Kächer, B., Koch, D., Kinne, S., Kondo, Y., Quinn, P. K., Sarofim, M. C., Schultz, M. G., Schulz, M., Venkataraman, C., Zhang, H., Zhang, S., Bellouin, N., Guttikunda, S. K., Hopke, P. K., Jacobson, M. Z., Kaiser, J. W., Klimont, Z., Lohmann, U., Schwarz, J. P., Shindell, D., Storelvmo, T., Warren, S. G., and Zender, C. S.: Bounding the role of black carbon in the climate system: A scientific assessment, J. Geophys. Res. Atmos., 118, 5380–5552, doi:10.1002/jgrd.50171, 2013.

Boos, W. R., and Kuang, Z.: Dominant control of the South Asian monsoon by orographic insulation versus plateau heating, Nature, 463, 218–222, 2010.

Colarco, P. R., Nowottnick, E. P., Randles, C. A., Yi, B., Yang, P., Kim, K.-M., Smith, J. A., and Bardeen, C. G.: Impact of radiatively interactive dust aerosols in the NASA GEOS-5 climate model: Sensitivity to dust particle shape and refractive index, J. Geophys. Res. Atmos., 119, 753–786, doi:10.1002/2013JD020046, 2014.

Dang, C., Q. Fu, and S. Warren: Effect of Snow Grain Shape on Snow Albedo, J. Atmos. Sci., 73, 3573–3583, doi: 10.1175/JAS-D-15-0276.1, 2016.

Flanner, M. G., Zender, C. S., Randerson, J. T., and Rasch, P. J.: Present day climate forcing and response from black carbon in snow, J. Geophys. Res., 112, D11202, doi:10.1029/ 2006JD008003, 2007.

Flanner, M. G., Zender, C. S., Hess, P. G., Mahowald, N. M., Painter, T. H., Ramanathan, V., and Rasch, P. J.: Springtime warming and reduced snow cover from carbonaceous particles, Atmos. Chem. Phys., 9, 2481–2497, doi:10.5194/acp-9-2481-2009, 2009.

Flanner, M. G., X. Liu, C. Zhou, J. E. Penner, and C. Jiao: Enhanced solar energy absorption by internally-mixed black carbon in snow grains, Atmos. Chem. Phys., 12(10), 4699–4721, doi:10.5194/acp-12-4699-2012, 2012.

Gu, Y., Xue, Y., De Sales, F., Liou, K. N.: A GCM investigation of dust aerosol impact on the regional climate of North Africa and South/East Asia, Clim. Dyn., 46, 2353–2370, 2016.

Guo, J., and Yin, Y.: Mineral dust impacts on regional precipitation and summer circulation in East Asia using a regional coupled climate system model, J. Geophys. Res. Atmos. 120, 10,378–10,398, doi:10.1002/2015JD023096, 2015.

Guo, J., Lou, M., Miao, Y., Wang, Y., Zeng, Z., Liu, H., He, J., Xu, H., Wang, F., Min, M., Zhai, P.: Trans-Pacific transport of dust aerosols from East Asia: Insights gained from multiple observations and modeling, Environ. Pollut., 230, 1030–1039, 2017.

Han, Z. W., Li, J. W., Xia, X. G., and Zhang, R. J.: Investigation of direct radiative effects of aerosols in dust storm season over East Asia with an online coupled regional climate-chemistry-aerosol model, Atmos. Environ., 54, 688–699, 2012.

Hansen, J. and Nazarenko, L.: Soot climate forcing via snow and ice albedos, P. Natl. Acad. Sci. USA, 101(2), 423–428, 2004.

Hansen, J., and Coauthors: Efficacy of climate forcings. J.Geophy. Res., 110, D18104, doi: 10.1029/2005JD005776, 2005.

He, C., Takano, Y., and Liou, K.-N.: Close packing effects on clean and dirty snow albedo and associated climatic implications, Geophys. Res. Lett., 44, doi:10.1002/2017GL072916, 2017a.

He, C., Takano, Y., Liou, K.-N., Yang, P., Li, Q., and Chen, F.: Impact of snow grain shape and black carbon-snow internal mixing on snow optical properties: Parameterizations for climate models. Journal of Climate, 30, 10,019–10,036, doi:10.1175/JCLI-D-17-0300.1, 2017b.

He, C., Liou, K.-N., Takano, Y., Yang, P., Qi, L., and Chen, F.: Impact of grain shape and multiple black carbon internal mixing on snow albedo: Parameterization and radiative effect analysis. J. Geophys. Res.-Atmos., 123, 1253-1268, doi:10.1002/2017JD027752, 2018a.

He, C., Liou, K.-N., and Takano, Y.: Resolving size distribution of black carbon internally mixed with snow: Impact on snow optical properties and albedo. Geophys. Res. Lett., 45, 2697–2705, doi:10.1002/2018GL077062, 2018b.

He, C., Flanner, M. G., Chen, F., Barlage, M., Liou, K.-N., Kang, S., Ming, J., and Qian, Y.: Black carbon-induced snow albedo reduction over the Tibetan Plateau: Uncertainties from snow grain shape and aerosol-snow mixing state based on an updated SNICAR model, Atmos. Chem. Phys. Discuss., doi:10.5194/acp-2018-476, in review, 2018c.

Heinold, B., Helmert, J., Hellmuth, O., Wolke, R., Ansmann, A., Marticorena, B., Laurent, B., and Tegen, I.: Regional modeling of Saharan dust events using LM-MUSCAT: Model description and case studies, J. Geophys. Res., 112, D11204, doi:10.1029/2006JD007443, 2007.

Heinold, B., Tegen, I., Schepanski, K., and Hellmuth, O.: Dust radiative feedback on Saharan boundary layer dynamics and dust mobilization, Geophys. Res. Lett., 35, L20817, doi:10.1029/2008GL035319, 2008.

Huang, J., Fu, Q., Zhang, W., Wang, X., Zhang, R., Ye, H., and Warren, S. G.: Dust and black carbon in seasonal snow across Northern China, Bull. Am. Meteorol. Soc., doi: 10.1175/2010BAMS3064.1, 2011.

Huang, J., Wang, T., Wang, W., Li, Z., Yan, H.: Climate effects of dust aerosols over East Asian arid and semiarid regions, J. Geophys. Res. Atmos., 119, 11, 398–11, 416, doi: 10.1002/2014JD021796, 2014.

Huneeus, N., Schulz, M., Balkanski, Y., Griesfeller, J., Prospero, J., Kinne, S., Bauer, S., Boucher, O., Chin, M., Dentener, F., Diehl, T., Easter, R., Fillmore, D., Ghan, S., Ginoux, P., Grini, A., Horowitz, L., Koch, D., Krol, M. C., Landing, W., Liu, X., Mahowald, N., Miller, R., Morcrette, J.-J., Myhre, G., Penner, J., Perlwitz, J., Stier, P., Takemura, T., and Zender, C. S.: Global dust model intercomparison in AeroCom phase I, Atmos. Chem. Phys., 11, 7781–7816, doi: 10.5194/acp-11-7781-2011, 2011.

Hurrell, J., Hack, J., Shea, D., Caron, J., and Rosinski, J.: A new sea surface temperature and sea ice boundary data set for the Community Atmosphere Model, J. Clim., 21(19), 5145–5153, doi:10.1175/2008JCLI2292.1, 2008.

IPCC: Climate Change 2007: The Physical Science Basis. Contribution of Working Group I to the Fourth Assessment Report of the Intergovernmental Panel on Climate Change, edited by: Solomon, S., Qin, D., Manning, M., Chen, Z., Marquis, M., Averyt, K. B., Tignor, M., and Miller, H. L., Cambridge University Press, 996 pp., 2007.

IPCC: Climate Change 2013: The Physical Science Basis. Contribution of Working Group I to the Fifth Assessment Report of the Intergovernmental Panel on Climate Change, edited by: Stocker, T. F., Qin, D., Plattner, G.-K., Tignor, M., Allen, S. K., Boschung, J., Nauels, A., Xia, Y., Bex, V., and Midgley, P. M., Cambridge University Press, Cambridge, United Kingdom and New York, NY, USA, 1535 pp., 2013.

Kang, S. C., Xu, Y. W., You, Q. L., Flugel, W., Pepin, N., and Yao, T. D.: Review of climate and cryospheric change in the Tibetan Plateau, Environ. Res. Lett., 5, 015101, 2010.

Kok, J. F.: A scaling theory for the size distribution of emitted dust aerosols suggests climate models underestimate the size of the global dust cycle, Proceedings of the National Academy of Sciences of the United States of America, 108, 1016–1021, https://doi.org/10.1073/pnas.1014798108, 2011.

Kok, J. F., Ridley, D. A., Zhou, Q., Miller, R. L., Zhao, C., Heald, C. L., Ward, D. S., Albani, S., Haustein, K.: Smaller desert dust cooling effect estimated from analysis of dust size and abundance, Nature Geosci., 10, 274–278, doi:10.1038/ngeo2912, 2017.

Lau, K. M., Kim, M. K., and Kim, K. M.:. Asian monsoon anomalies induced by aerosol direct forcing: the role of the Tibetan Plateau, Clim. Dyn., 26, 855–664, 2006.

Lau, K.-M., Kim, M. K., Kim, K.-M., and Lee, W. S.: Enhanced surface warming and accelerated snow melt in the Himalayas and Tibetan Plateau induced by absorbing aerosols, Environ. Res. Lett., 5, 025204 doi:10.1088/1748-9326/5/2/025204, 2010.

Lee, W. S., Bhawar, R. L., Kim, M. K., and Sang, J.: Study of aerosol effect on accelerated snow melting over the Tibetan Plateau during boreal spring, Atmos. Environ., 75, 113-122, 2013.

Lee, W.-L., Liou, K. N., He, C., Liang, H.-C., Wang, T.-C., Li, Q., Liu, Z., and Yue, Q.: Impact of absorbing aerosol deposition on snow albedo reduction over the southern Tibetan plateau based on satellite observations, Theor. Appl. Climatol., 129(3-4), 1373–1382, doi:10.1007/s00704-016-1860-4, 2017.

Li, J., Yu, R., Yuan, W., Chen, H., Sun, W., and Zhang Y.: Precipitation over East Asia simulated by NCAR CAM5 at different horizontal resolutions, J. Adv. Model. Earth Syst., 7, 774–790, doi:10.1002/2014MS000414, 2015.

Li, X., Kang, S., Zhang, G., Que, B., Tripatheea, L., Paudyal, R., Jing, Z., Zhang, Y., Yan, F., Li, G., Cui, X., Xu, R., Hu, Z., and Li, C.: Light-absorbing impurities in a southern Tibetan Plateau glacier: Variations and potential impact on snow albedo and radiative forcing, Atmos. Res., 200, 77–87, doi:10.1016/j.atmosres.2017.10.002, 2018.

Li, X. Z., and Liu, X. D.: Numerical simulation of Tibetan Plateau heating anomaly influence on westerly jet in spring, J. Earth Syst. Sci. 124, 1599–1607, 2015.

Li, Y., Wang, T., Zeng, Z., Peng, S., Lian, X., and Piao, S.: Evaluating biases in simulated land surface albedo from CMIP5 global climate models, J. Geophys. Res. Atmos., 121, 6178–6190, doi:10.1002/2016JD024774, 2016.

Liou, K. N., Takano, Y., He, C., Yang, P., Leung, R. L., Gu, Y., and Lee, W. L.: Stochastic parameterization for light absorption by internally mixed BC/dust in snow grains for application to climate models, J. Geophys. Res.-Atmos., 119, 7616–7632, doi:10.1002/2014JD021665, 2014.

Liu, X., and Dong, B.: Influence of the Tibetan Plateau uplift on the Asian monsoon-arid environment evolution, Chin. Sci. Bull., 58, 4277–4291, doi:10.1007/s11434-013-5987-8, 2013.

Mahowald, N. M., Muhs, D. R.,Levis, S., Rasch, P. J., Yoshioka, M., Zender, C. S., and Luo C.: Change in atmospheric mineral aerosols in response to climate: Last glacial period, preindustrial, modern, and doubled carbon dioxide climates, J. Geophys. Res., 111, D10202, doi:10.1029/2005JD006653, 2006.

Mahowald, N. M., Albani, S., Kok, J. F., Engelstaedter, S., Scanza, R., Ward, D. S., Flanner, M. G.: The size distribution of desert dust aerosols and its impact on the Earth system, Aeolian Res. 15, 53–71. http://dx.doi.org/10.1016/j.aeolia.2013.09.002, 2014.

Maher, B. A., Prospero, J. M., Mackie, D., Gaiero, D., Hesse, P., Balkanski, Y.: Global connections between aeolian dust, climate and ocean biogeochemistry at the present day and at the last glacial maximum, earth-sci. rev., 99, 61–97, doi:10.1016/j.earscirev.2009.12.001, 2010.

Meng, X., Lyu, S., Zhang, T., Zhao, L., Li, Z., Han, B., Li, S., Ma, D., Chen, H., Ao, Y., Luo, S., Shen, Y., Guo, J., and Wen, L.: Simulated cold bias being improved by using MODIS time-varying albedo in the Tibetan Plateau in WRF model, Environ. Res. Lett. 13, 044028, 2018.

Miller, R. L., and Tegen, I.: Climate response to soil dust aerosols, J. Clim., 11, 3247–3267, 1998.

Ming, J., Wang, P., Zhao, S., and Chen, P.: Disturbance of light-absorbing aerosols on the albedo in a winter snowpack of Central Tibet, Journal of Environmental Sciences-China, 25(8), 1601–1607, doi: 10.1016/S1001-0742(12)60220-4, 2013.

Neale, R. B., et al.: Description of the NCAR Community Atmosphere Model (CAM 4.0), NCAR Tech. Note, TN–485, pp. 212, Natl. Cent. for Atmos. Res., Boulder, Colo, 2010.

Perez, C., Nickovic, S., Pejanovic, G., Baldasano, J. M., and Ozsoy, E.: Interactive dust-radiation modeling: A step to improve weather forecasts, J. Geophys. Res., 111, D16206, doi:10.1029/2005JD006717, 2006.

Perlwitz, J. P., Tegen, I., and Miller, R. L.: Interactive soil dust aerosol model in the GISS GCM: 1. Sensitivity of the soil dust cycle to radiative properties of soil dust aerosols, J. Geophys. Res., 106, 18167–18192, doi:10.1029/2000JD900668, 2001.

Pu, Z., Xu, L., Salomonson, V. V.: MODIS/Terra observed seasonal variations of snow cover over the Tibetan Plateau, Geophys. Res. Lett., 34, L06706, doi: 10.1029/2007GL029262, 2007.

Qian, Y., Flanner, M., Leung, L., and Wang, W.: Sensitivity studies on the impacts of Tibetan Plateau snowpack pollution on the Asian hydrological cycle and monsoon climate, Atmos. Chem. Phys., 11(5), 1929–1948, doi: 10.5194/acp-11-1929-2011, 2011.

Qian, Y., Yasunari, T. J., Doherty, S. J., Flanner, M. G., Lau, W. K. M., Jing, M., Wang, H., Wang, M., Warren, S. G., and Zhang, R.: Light-absorbing Particles in Snow and Ice: Measurement and Modeling of Climatic and Hydrological impact, Adv. Atmos. Sci., 32, 64–91, doi:10.1007/s00376-014-0010-0, 2015.

Qu, B., Ming, J., Kang, S.-C., Zhang, G.-S., Li, Y.-W., Li, C.-D., Zhao, S.-Y., Ji, Z.-M., and Cao, J.-J.: The decreasing albedo of Zhadang glacier on western Nyainqentanglha and the role of lightabsorbing impurities, Atmos. Chem. Phys., 14, 11117–11128, doi:10.5194/acp-14-11117-2014, 2014.

Ramanathan, V., Crutzen, P. J., Kiehl, J. T. and Rosenfeld, D.: Aerosols, climate, and the hydrological cycle, Science, 294, 2119–2124, 2001.

Rayner, N. A., Parker, D. E., Horton, E. B., Folland, C. K., Alexander, L. V., Rowell, D. P., Kent, E. C., and Kaplan, A.: Global analyses of sea surface temperature, sea ice, and night marine air temperature since the late nineteenth century, J. Geophys. Res., 108(D14), 4407, doi:10.1029/2002JD002670, 2003.

Schiemann, R., Lüthi, D., Schär, C.: Seasonality and interannual variability of the westerly jet in the Tibetan Plateau region, J. Clim. 22, 2940–2957, 2009.

Schwarz, J. P., Gao, R. S., Perring, A. E., Spackman, J. R., and Fahey, D. W.: Black carbon aerosol size in snow. Scientific Reports, 3(1), 1356, 2013.

Shao, Y., Wyrwoll, K. H., Chappell, A., Huang, J., Lin, Z., McTainsh, G. H., Mikami, M., Tanaka, T. Y., Wang, X., and Yoon, S.: Dust cycle: an emerging core theme in Earth System Science, Aeolian Res., 2, 181–204, 2011.

Sha, Y., Shi, Z., Liu, X., and An, Z.: Distinct impacts of the Mongolian and Tibetan Plateaus on the evolution of the East Asian monsoon, J. Geophys. Res. Atmos., 120, 4764–4782, doi:10.1002/2014JD022880, 2015.

Shi, Z., Liu, X., Liu, Y., Sha, Y., and Xu, T.: Impact of Mongolian Plateau versus Tibetan Plateau on the westerly jet over North Pacific Ocean, Clim. Dyn., 42, 1–10, doi:10.1007/s00382-014-2217-2, 2014.

Sun, H., Pan, Z., and Liu, X.: Numerical simulation of spatial-temporal distribution of dust aerosol and its direct radiative effects on East Asian climate, J. Geophys. Res., 117, D13206, doi:10.1029/2011JD017219, 2012.

Sun, H., and Liu, X.: Numerical simulation of the direct radiative effects of dust aerosol on the East Asian winter monsoon, Adv. Meteorol., 2015, 142617, doi:10.1155/2015/142617, 2015.

Tegen, I., and Lacis A. A.: Modeling of particle size distribution and its influence on the radiative properties of mineral dust aerosol, J. Geophys. Res., 101(D14), 19237–19244, 1996.

Tie, X., Madronich, S., Walters, S., Edwards, D. P., Ginoux, P., Mahowald, N., Zhang, R., Lou, C., and Brasseur, G.: Assessment of the global impact of aerosols on tropospheric oxidants, J. Geophys. Res.-Atmos., 110, https://doi.org/10.1029/2004JD005359, 2005.

Wake, C. P., Mayewsi, P. A., Li, Z., Han, J., and Qin, D.: Modern eolian dust deposition in central Asia, Tellus, 46B, 220–233, 1994.

Wang, M., Xu, B., Cao, J., Tie, X., Wang, H., Zhang, R., Qian, Y., Rasch, P. J., Zhao, S., Wu, G., Zhao, H., Joswiak, D. R., Li, J., and Xie, Y.: Carbonaceous aerosols recorded in a southeastern Tibetan glacier: analysis of temporal variations and model estimates of sources and radiative forcing, Atmos. Chem. Phys., 15, 1191–1204, https://doi.org/10.5194/acp-15-1191-2015, 2015.

Wilkening, K. E., Barrie, L. A., Engle, M.: Trans-Pacific air pollution, Science, 290, 65–67. http://dx.doi.org/10.1126/science.290.5489.65, 2000.

Wu, G. X., Liu, Y. M., He, B., Bao, Q., Duan, A. M., Jin, F. F.: Thermal controls on the Asian summer monsoon, Sci. Rep., 2, 1–7, 2012.

Xie, X. N., Liu, X. D., Che, H. Z., Xie, X. X., Wang, H. L., Li, J. D., Shi, Z. G., and Liu, Y.: Modeling East Asian dust and its radiative feedbacks in CAM4-BAM, J. Geophys. Res. Atmos., 123, 1079–1096, https://doi.org/10.1002/2017JD027343, 2018.

Xu, B. Q., Cao, J., Hansen, J., Yao, T., Joswiak, D. R., Wang, N., Wu, G.,Wang, M., Zhao, H., Yang,W., Liu, X., and He, J.: Black soot and the survival of Tibetan glaciers, P. Natl. Acad. Sci. USA, 106(52), 22114–22118, doi:10.1073/pnas.0910444106, 2009.

Xu, Z. X., Gong, T. L., and Li, J. Y.: Decadal trend of climate in the Tibetan Plateau-regional temperature and precipitation, Hydrol. Process. 22, 3056–3065, 2008.

Yue, X., Wang, H., Wang, Z., and Fan, K.: Simulation of dust aerosol radiative feedback using the Global Transport Model of Dust: 1. Dust cycle and validation, J. Geophys. Res., 114, D10202, doi:10.1029/2008JD010995, 2009.

Zhang, D. F., Zakey, A. S., Gao, X. J., Giorgi, F., and Solmon, F.: Simulation of dust aerosol and its regional feedbacks over East Asia using a regional climate model, Atmos. Chem. Phys., 9, 1095–1110, doi:10.5194/acp-9-1095-2009, 2009.

Zhang, X. Y., Arimoto, R., An, Z. S.: Dust emission from Chinese desert sources linked to variations in atmospheric circulation, J. Geophys. Res., 102(DD23), 28, 041–28, 047, 1997.

Zhang, Y., Kang, S., Sprenger, M., Cong, Z., Gao, T., Li, C., Tao, S., Li, X., Zhong, X., Xu, M., Meng, W., Neupane, B., Qin, X., and Sillanpää, M.: Black carbon and mineral dust in snow cover on the Tibetan Plateau, The Cryosphere, 12, 413–431, doi:10.5194/tc-12-413-2018, 2018.

Zhao, T. L., Gong, S. L., Zhang, X. Y., Blanchet, J. P., McKendry, I. G., Zhou, Z. J.: A simulated climatology of Asian dust aerosol and its trans-Pacific transport, Part I: Mean climate and validation. J. Clim. 19, 88–103, 2006.

Table 1. Description of the Model experiments in this work. Here DRF represents dust direct radiative forcing and SRF is defined as dust-in-snow radiative forcing.

Experiments	Simulated time	DRF	SRF
Case1	21 years (1 years spinup)	Yes	Yes
Case2	21 years (1 years spinup)	Yes	No
Case3	21 years (1 years spinup)	No	No

Table 2. The March-April-May (MAM) averaged dust emissions (Tg season^{-1}) , transport (g m^{-1} s^{-1}), dry deposition (Tg season^{-1}), and wet deposition (Tg season^{-1}) over the East Asian dust source area (75°E−115°E and 25°N−50°N) in Case1, Case2, and Case3, as well as their corresponding differences between these three experiments.

	Dust emission	Dust transport	Dry deposition	Wet deposition
Case1	122.40	1.08	68.92	36.99
Case2	107.62	1.01	61.59	35.33
Case3	116.42	1.09	65.33	35.96
DRF (Case2−Case3)	−8.80 (−7.6%)	−0.07 (−6.4%)	−3.74 (−5.7%)	−0.63 (−1.8%)
SRF (Case1−Case2)	14.78 (13.7%)	0.07 (6.9%)	7.33 (11.9%)	1.66 (4.7%)
DRF+SRF (Case1−Case3)	5.98 (5.1%)	−0.01 (−0.9%)	3.59 (5.5%)	1.03 (2.9%)

Table 3. The March-April-May (MAM) averaged dust emissions (Tg season^{-1}) , transport (g m^{-1} s^{-1}), dry deposition (Tg season^{-1}), and wet deposition (Tg season^{-1}) over the North African dust source area ($-20°$E$-35°$E and $10°$N$-30°$N) in Case1, Case2, and Case3, as well as their corresponding differences between these three experiments.

	Dust emission	Dust transport	Dry deposition	Wet deposition
Case1	276.21	2.70	177.28	16.21
Case2	292.21	2.84	187.23	16.51
Case3	268.34	2.79	168.54	14.73
DRF (Case2−Case3)	23.87 (8.9%)	0.05 (1.8%)	18.69 (11.1%)	1.78 (12.1%)
SRF (Case1−Case2)	−16.00 (−5.5%)	−0.14(−4.9%)	−9.95 (−5.3%)	−0.30 (1.8%)
DRF+SRF (Case1−Case3)	7.87 (2.93%)	−0.09 (−3.2%)	8.74 (5.2%)	1.48 (10.0%)

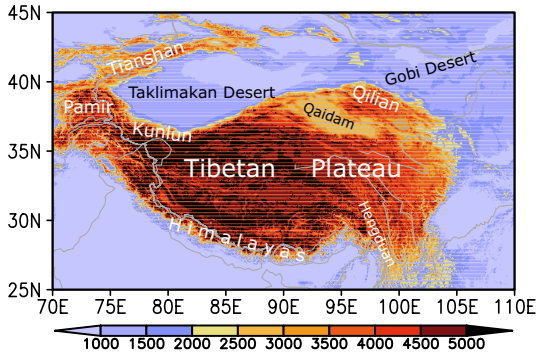

Figure 1. Terrain of the Tibetan Plateau (unit: m) including major mountains (Kunlun, Himalayas, Hengduan, Qilian and Tianshan Mountains), Pamir Plateau, Qaidam Basin deserts and its surrounding deserts (Taklimakan and Gobi deserts).

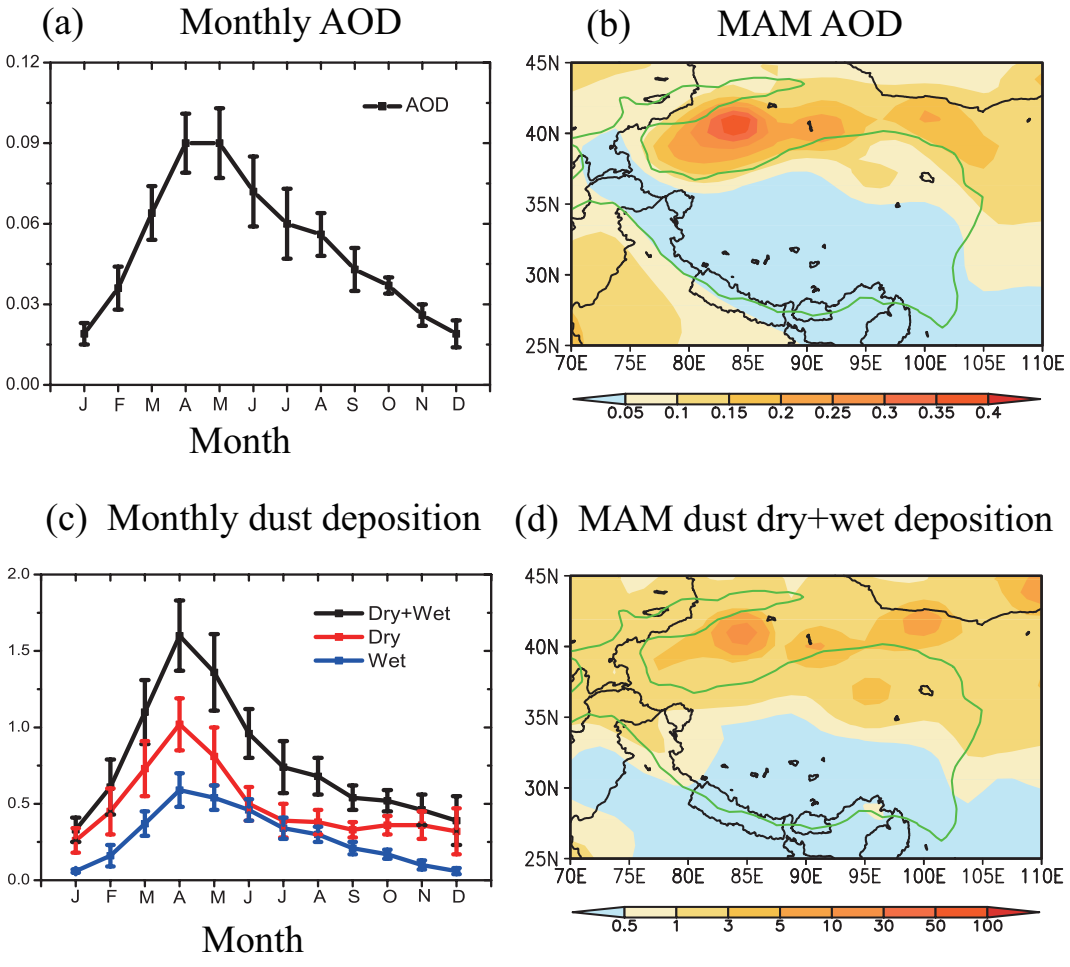

Figure 2. (a) Monthly dust AOD and spatial distribution of the March-April-May (MAM) averaged AOD from the CAM4-BAM model over the Tibetan Plateau (70°E−110°E and 25°N−45°N); (c) Monthly dust deposition (μg m^{-2} s^{-1}) including dust dry, wet and dry+wet deposition and (d) spatial distribution of the MAM averaged total dust deposition (dry+wet, μg m^{-2} s^{-1}) over this region. Note that the error bars (a, c) represent the standard deviation of the corresponding variables, and the green-contour area (b, d) indicates the plateau above 2500 m.

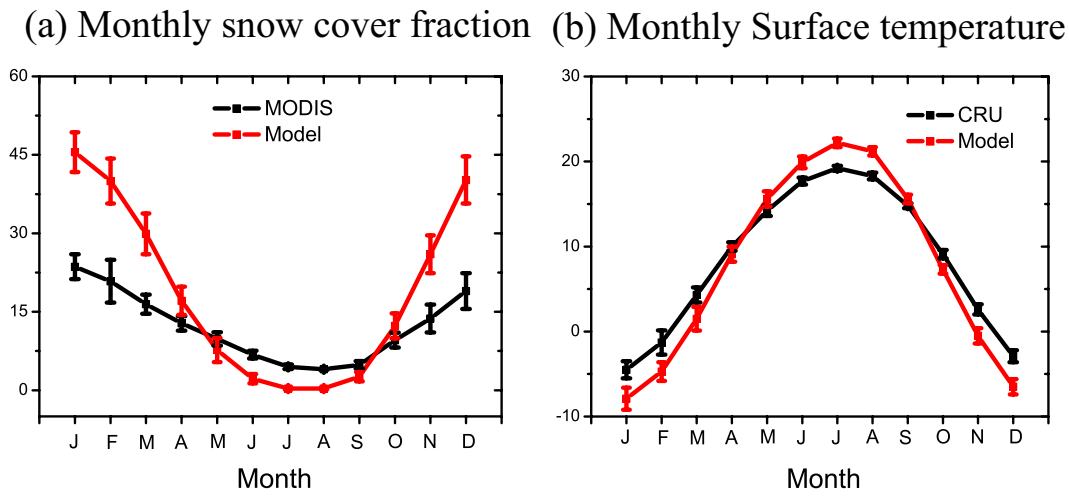

Figure 3. (a) Monthly snow cover fraction (%) from MODIS and Model; (b) monthly surface temperature (°C) from CRU and Model over the Tibetan Plateau (25N−45N, 70E−110E), where the error bars represent the standard deviation of the corresponding variables.

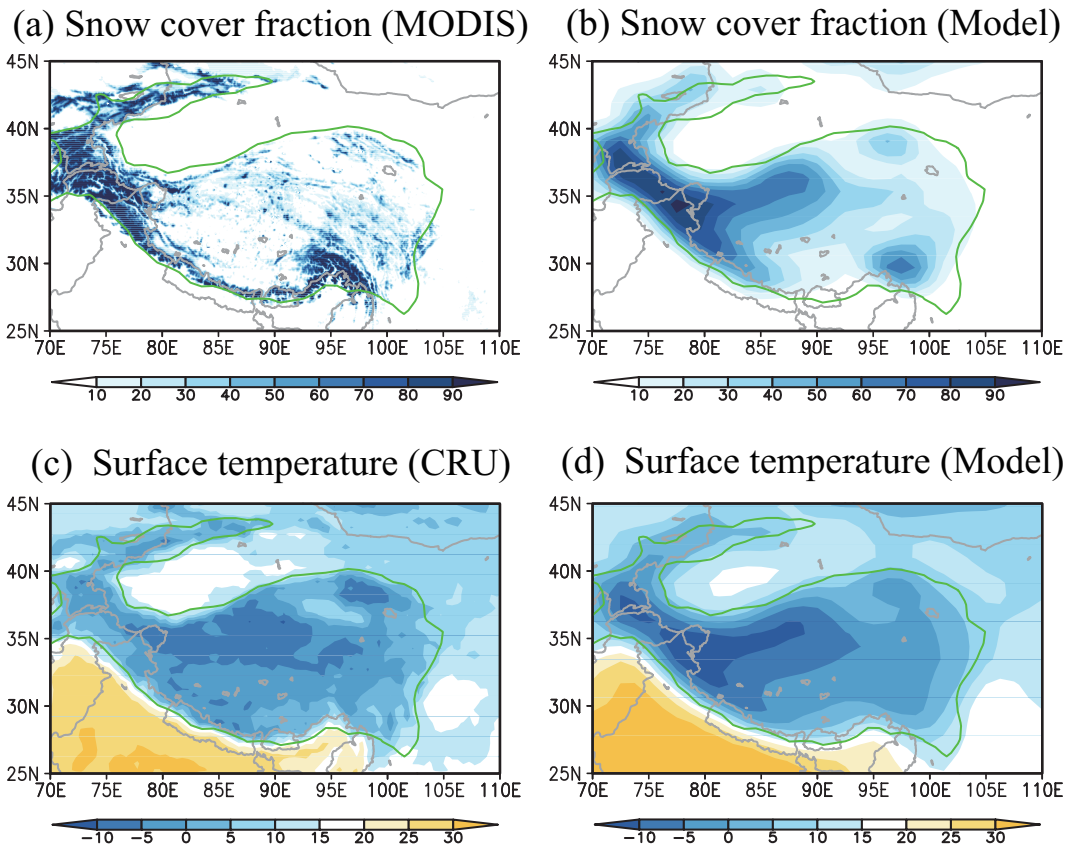

Figure 4. Spatial distribution of the MAM averaged (a) snow cover fraction (%) derived from MODIS for 2002−2012 and (c) surface temperature (°C) from CRU for 1979−2012, compared with the simulated MAM averaged (b) snow cover and (d) surface temperature for 20 model years over Tibetan Plateau. The green-contour area indicates the plateau above 2500 m.

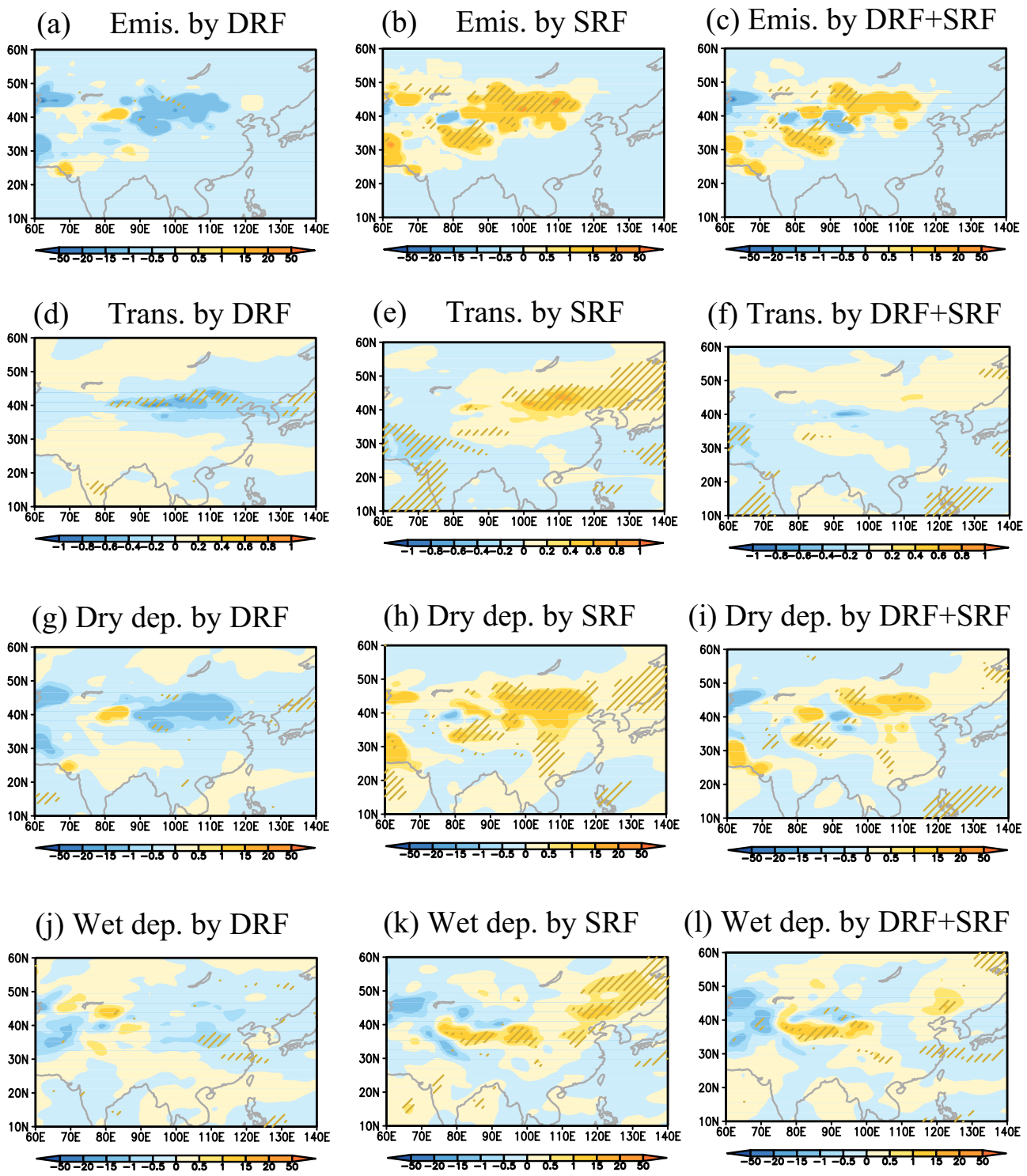

Figure 5. Dust cycle changes including (a, b, and c) dust emissions (g m^{-2} $season^{-1}$), (d, e, and f) dust transport (g m^{-1} s^{-1}), (g, h, and i) dust dry deposition (g m^{-2} $season^{-1}$), and (j, k, and l) dust wet deposition (g m^{-2} $season^{-1}$) in MAM induced by dust direct radiative forcing (DRF), dust-in-snow radiative forcing (SRF), and total forcing (DRF+SRF). The oblique line represents the grid points where the changes pass the two-tailed t-test at the 5% significance level.

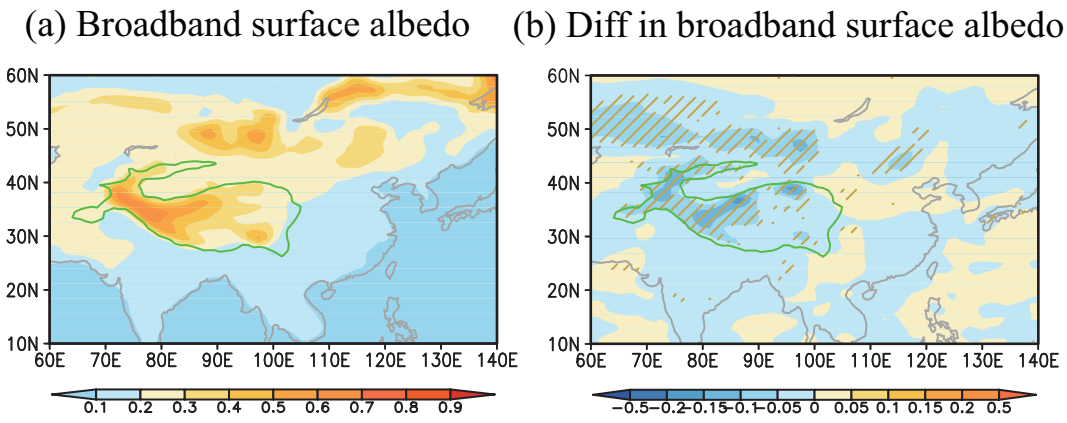

Figure 6. (a) Spatial distribution of the broadband surface albedo in MAM (Case 1) and (b) its changes between Case 1 and Case2, which are induced by dust-in-snow radiative forcing (SRF). The oblique line represents the grid points where the changes pass the two-tailed t-test at the 5% significance level. The green-contour area indicates the plateau above 2500 m.

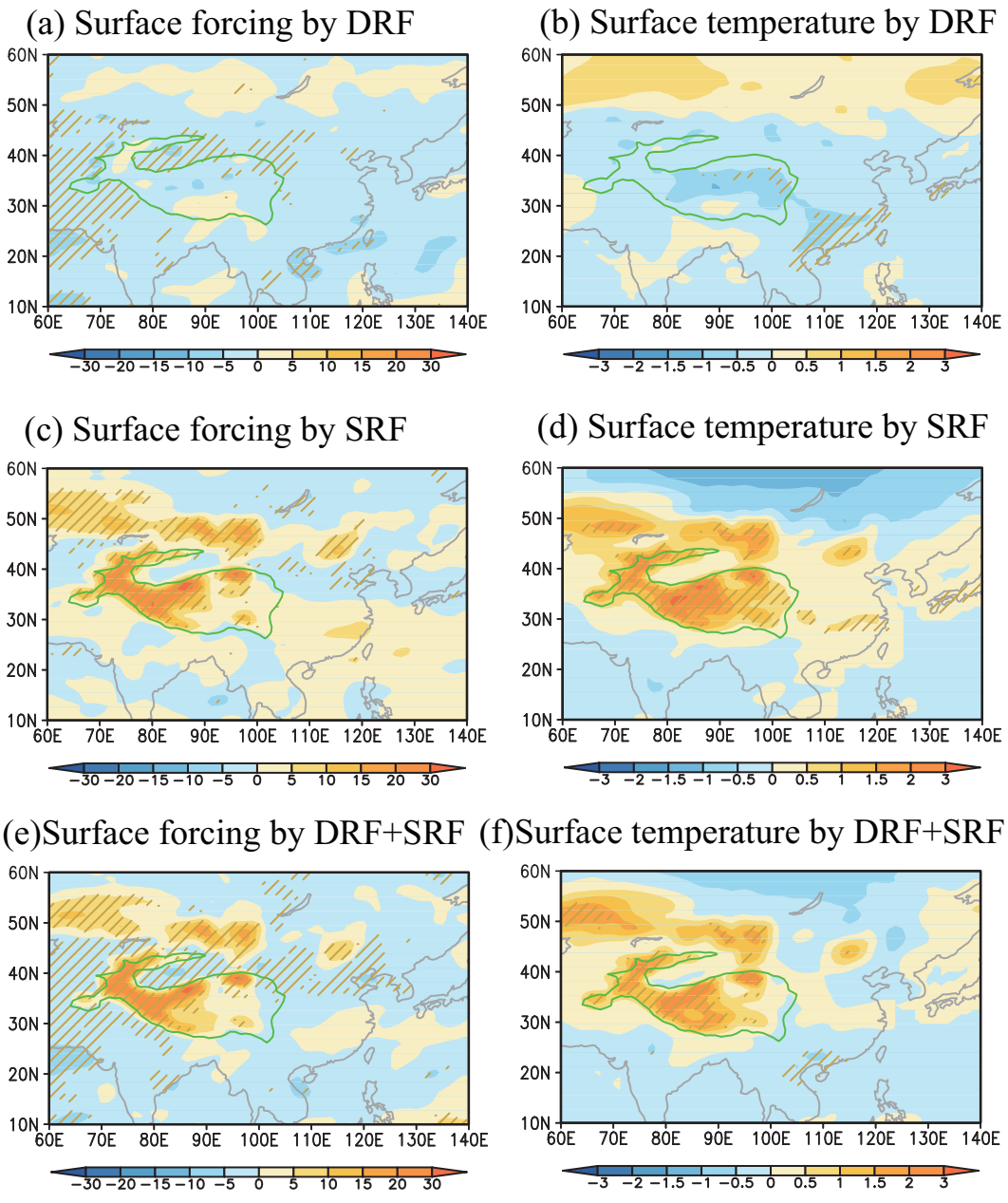

Figure 7. Spatial distribution of the changes in (a, c, e) the surface radiative forcing (W m^{-2}), (b, d, f) the surface temperature (°C) in MAM induced by dust direct radiative forcing (DRF), dust-in-snow radiative forcing (SRF), and total radiative forcing (DRF+SRF). The oblique line represents the grid points where the changes pass the two-tailed t-test at the 5% significance level. The green-contour area indicates the plateau above 2500 m.

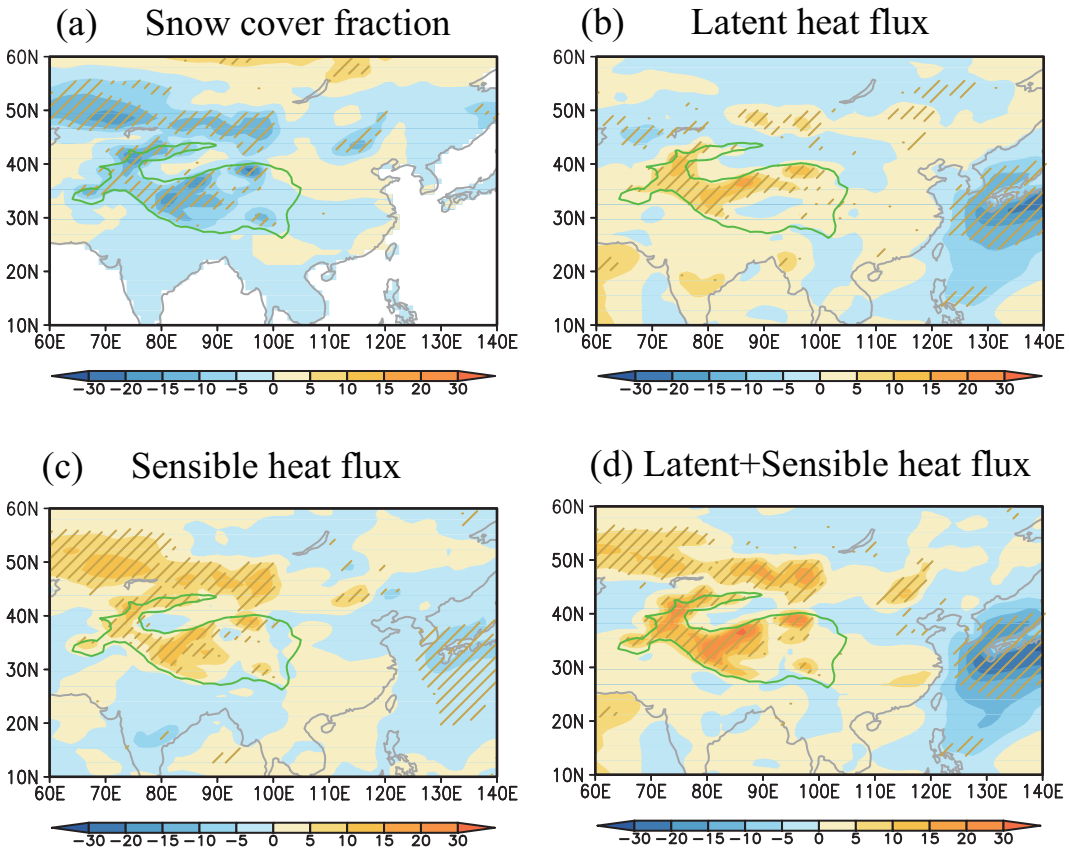

Figure 8. Spatial distribution of the changes in (a) the snow cover fraction (%), (b) the surface latent heat flux (W m^{-2}), (c) the surface sensible heat flux (W m^{-2}), and (d) the surface latent+sensible heat flux (W m^{-2}) in MAM induced by the dust-in-snow radiative forcing. Here the oblique line or the grey shaded area represent the grid points where the changes pass the two-tailed t-test at the 5% significance level. The green-contour area indicates the plateau above 2500 m.

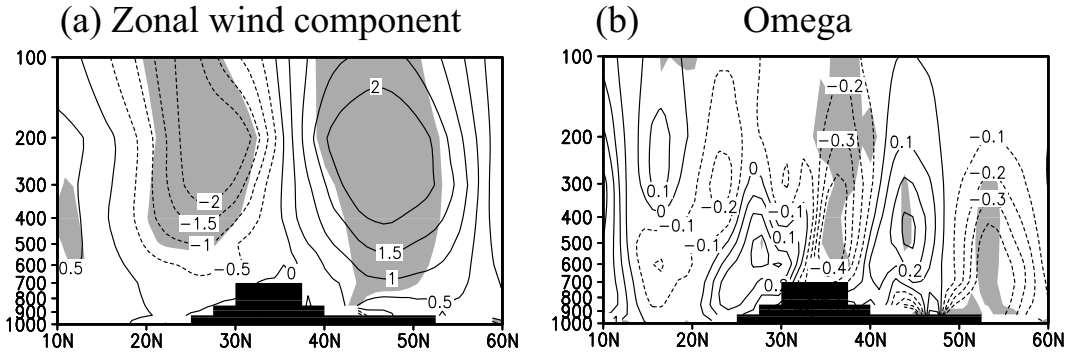

Figure 9. Changes in (a) the zonal wind component (m s^{-1}) and (b) the Omega (0.01 $\times$ Pa s^{-1}) in a vertical cross section at 75°E−115°E in MAM induced by the dust-in-snow radiative forcing. Here the grey shaded area represents the grid points where the changes pass the two-tailed t-test at the 5% significance level. The black shaded area indicates the plateau topography.

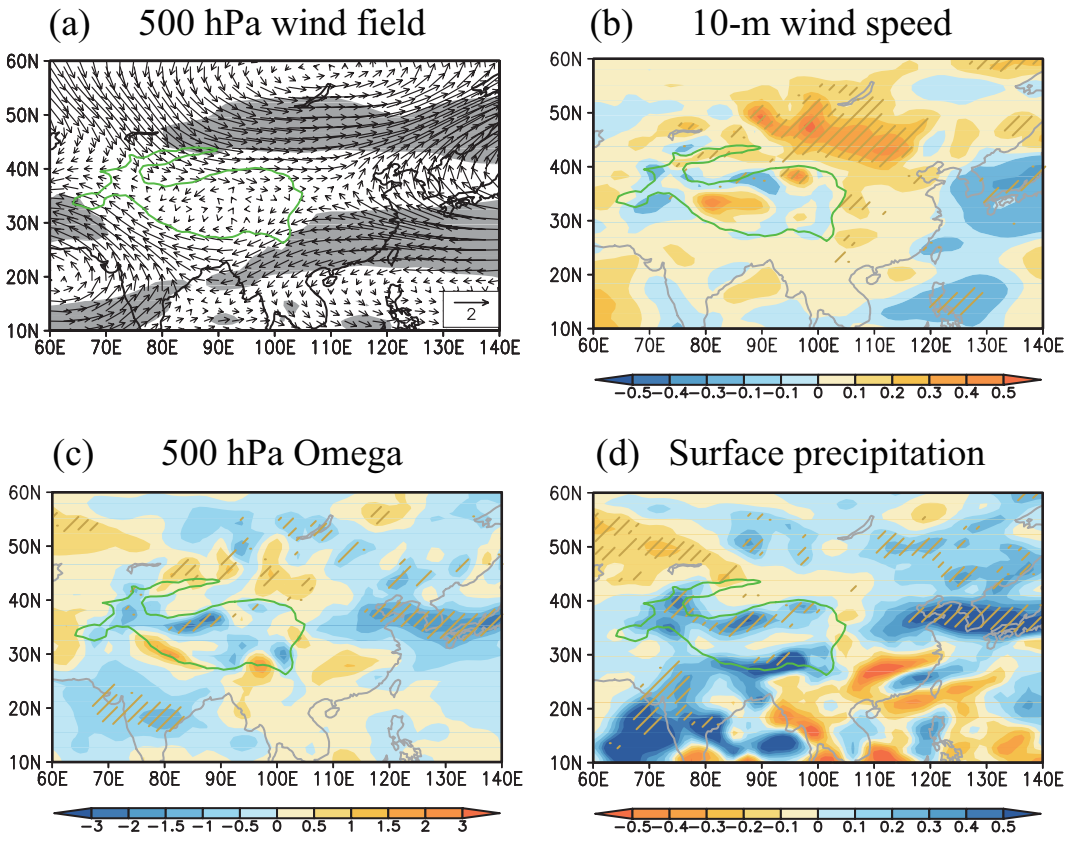

Figure 10. Spatial distribution of the changes in (a) the 500 hPa wind field (m s^{-1}), (b) the 10-m wind speed (m s^{-1}), (c) the 500 hPa Omega (0.01 $\times$ Pa s^{-1}), and (d) the surface precipitation (mm day^{-1}) in MAM induced by the dust-in-snow radiative forcing. Here the oblique line or the grey shaded area represent the grid points where the changes pass the two-tailed t-test at the 5% significance level. The green-contour area indicates the plateau above 2500 m.

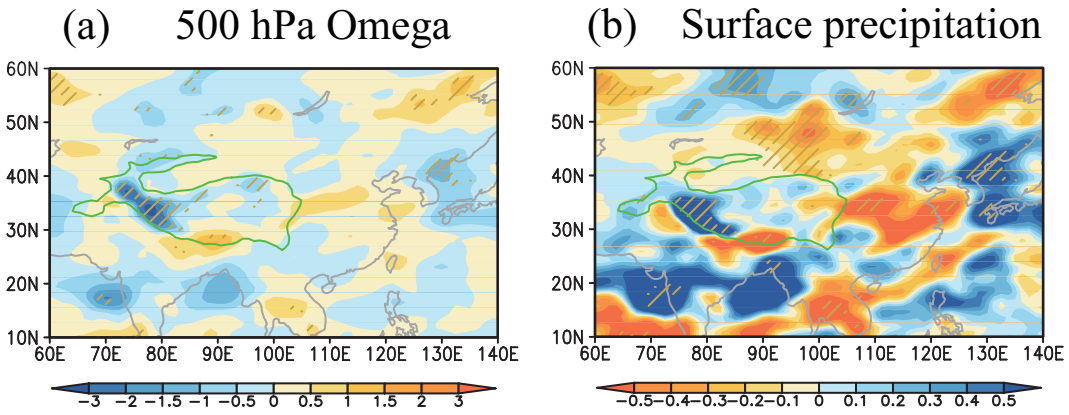

Figure 11. Spatial distribution of the changes in (a) the 500 hPa Omega ($0.01 \times$ Pa s^{-1}) and (b) the surface precipitation (mm day^{-1}) in June-July-August (JJA) induced by the dust-in-snow radiative forcing. The oblique line represents the grid points where the changes pass the two-tailed t-test at the 5% significance level. The green-contour area indicates the plateau above 2500 m.

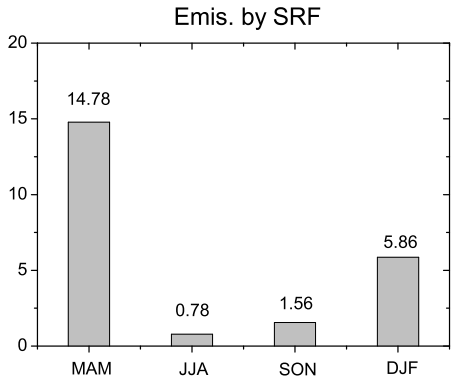

Figure 12. Seasonal changes in dust emissions (Tg season^{-1}) induced by the dust-in-snow radiative forcing (SRF) including March-April-May (MAM), June-July-August (JJA), September-October-November (SON), and December-January-February (DJF).

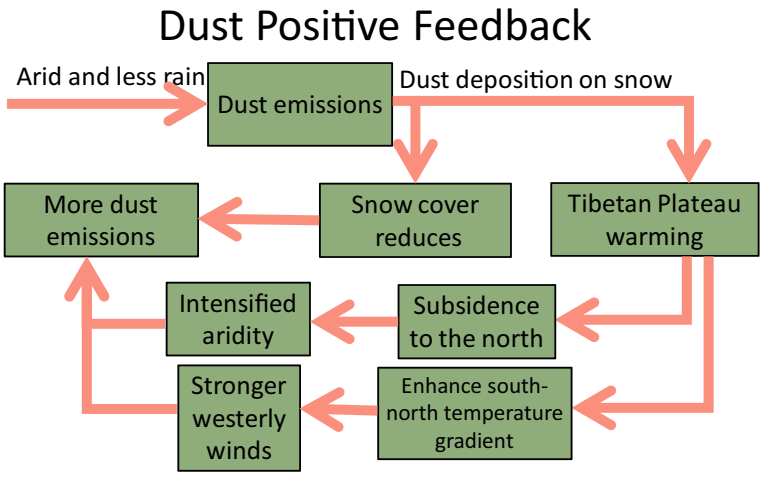

Figure 13. A schematic depiction of the feedback mechanism between dust emission and dust-in-snow radiative forcing.